

## 9-Iodoso-10-phenanthroate: Structure and Phosphoryltyc Properties of a Nonplanar Iodoxolone<sup>†</sup>

Robert A. Moss,\* Kathryn Bracken, and T. J. Emge

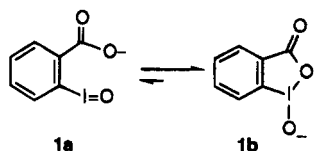
Department of Chemistry, Rutgers, The State University of New Jersey,  
New Brunswick, New Jersey 08903

Received July 5, 1995<sup>©</sup>

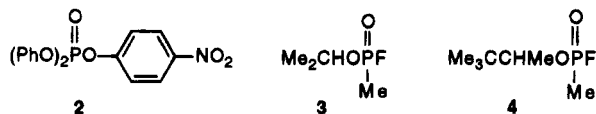
9-Iodoso-10-phenanthroic acid (IPA-OH) was prepared from 9-cyanophenanthrene in a four-step, 44% overall yield synthesis, featuring cyano-directed ortho lithiation/iodination as the key step. An X-ray crystal structure showed that IPA-OH exists in a phenanthroidoxol-3(1*H*)-one valence tautomeric form, 14-OH, characterized by T-shaped geometry at iodine, strong H/O steric interactions between the *peri*-H atoms and the carbonyl and iodoso oxygen atoms, a "short" endocyclic I–O bond, well-differentiated carbonyl and endocyclic C–O bond lengths, and nonplanarity in both the iodoxolone and phenanthrene rings (Figures 1 and 2). IPA-OH was an excellent catalyst for the cleavage of *p*-nitrophenyl diphenyl phosphate (PNPDPP) in aqueous micellar cetyltrimethylammonium chloride (CTACl) solutions at pH 8 and 25 °C:  $1 \times 10^{-5}$  M PNPDPP was cleaved by  $1 \times 10^{-4}$  M IPA-OH in  $3.5 \times 10^{-4}$  M CTACl with  $k_p = 0.38 \text{ s}^{-1}$ . Experiments in which  $[\text{PNPDPP}] > [\text{IPA-OH}]$  demonstrated that the catalyst "turned over"; hydrolysis of the putative phosphorylated IPA-OH intermediate was rapid.

### Background

The insane deployment of the nerve gas sarin in the Tokyo subways, and the tragic consequences,<sup>1</sup> powerfully demonstrates our continuing need for rapidly acting and efficient decontaminants against toxic phosphonates.<sup>2</sup> *o*-Iodosobenzoate, **1a**, is an effective decontaminant, which in its preferred oxido-1,2-benziodoxol-3(1*H*)-one valence tautomeric form, **1b**, catalyzes the hydrolytic cleavage of reactive phosphates and phosphonates.<sup>3</sup> Thus, dilute solutions of iodosobenzoate (IBA) in micellar

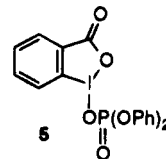


cetyltrimethylammonium chloride (CTACl) at pH 7.5–8 efficiently cleave the simulant substrate *p*-nitrophenyl diphenyl phosphate (**2**, PNPDPP)<sup>3</sup> and, more importantly, detoxify the fluorophosphonate nerve agents sarin (**3**) and soman (**4**).<sup>4</sup>



Mechanistically, IBA appears to function in a two-step sequence. Its nucleophilic I–O<sup>−</sup> moiety first attacks the substrate's phosphoryl group with the expulsion of *p*-

nitrophenylate ion (from **2**) or fluoride (from **3** or **4**) and the formation of a phosphorylated iodoxolone intermediate (e.g., **5** from substrate **2**).<sup>3b</sup> In the subsequent



(turnover) step, the intermediate is rapidly cleaved by OH<sup>−</sup> attack *directly at iodine*,<sup>5</sup> reforming IBA for renewed reaction with additional substrate molecules. Intermediate **5** can be independently prepared and does indeed undergo very rapid reactions with various nucleophiles (including water) at its iodine atom.<sup>6</sup>

The catalytic ability of IBA therefore depends on the rapid turnover of the phosphorylated intermediate in the second step of the reaction sequence, but the reagent's overall reactivity reflects the nucleophilicity of its I–O<sup>−</sup> unit, which is responsible for the initial attack on the substrate's P=O group. Accordingly, interest has focused on structure and bonding<sup>7</sup> in IBA and their relation to its nucleophilicity. One must also note that the intrinsic reactivity of the IBA requires a micellar environment for its expression. The cationic micellar CTACl brings the substrate and the IBA into close proximity in the micellar pseudophase. Additionally, it lowers the p*K*<sub>a</sub> of the IBA, increasing the concentration of its reactive anionic form. In the absence of CTACl, nonmicellar catalysis by IBA is minimal and the reaction is slow.<sup>3a</sup>

X-ray crystal structures of iodosobenzoic acid<sup>8</sup> and its 5-methyl derivative<sup>9</sup> reveal planar iodoxolone rings, "T-

<sup>†</sup> The author has deposited atomic coordinates for this structure with the Cambridge Crystallographic Data Centre. The coordinates can be obtained, on request, from the Director, Cambridge Crystallographic Data Centre, 12 Union Rd., Cambridge CB2 1E2, U.K.

<sup>©</sup> Abstract published in *Advance ACS Abstracts*, November 1, 1995.

(1) Kristof, N. D. *The New York Times* **1995**, *144*, (Tuesday, March 21), 1. Ember, L. *Chem. Eng. News* **1995** (March 27), 6.

(2) Yang, Y.-C.; Baker, J. A.; Ward, J. R. *Chem. Rev.* **1992**, *92*, 1729.

(3) (a) Moss, R. A.; Alwis, K. W.; Bizzigotti, G. *J. Am. Chem. Soc.* **1983**, *105*, 681. (b) Moss, R. A.; Alwis, K. W.; Shin, J.-S. *Ibid.* **1984**, *106*, 2651. (c) Moss, R. A.; Kim, K. Y.; Swarup, S. *Ibid.* **1986**, *108*, 788.

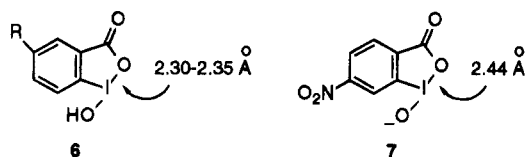
(4) Hammond, P. S.; Forster, J. S.; Lieske, C. N.; Durst, H. D. *J. Am. Chem. Soc.* **1989**, *111*, 7860.

(5) Moss, R. A.; Scrimin, P.; Rosen, R. T. *Tetrahedron Lett.* **1987**, *28*, 251.

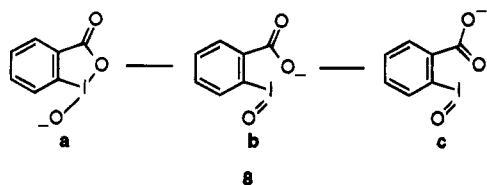
(6) Moss, R. A.; Zhang, H. *J. Am. Chem. Soc.* **1994**, *116*, 4471.

(7) Reviews: (a) Koser, G. F. In *The Chemistry of Functional Groups*, Supplement D; Patai, S., Rappoport, Z., Eds.; Wiley: New York, 1983; pp 721 f. (b) Varvoglis, A. *The Organic Chemistry of Polycordinated Iodine*; VCH Publishers, Inc.: New York, 1992; pp 168 f. (c) Nguyen, T. T.; Martin, J. C. In *Comprehensive Heterocyclic Chemistry*; Meth-Cohn, O., Ed.; Pergamon: Oxford, 1984; Vol. 1, pp 563 f.

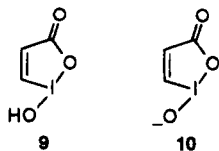
shaped" geometry at iodine (where the O–I–O bond angle is  $\sim 170^\circ$ ), and an endocyclic I–O bond that is considerably longer than the I–O single bond predicted from the sum ( $\sim 2.07$  Å) of the I and O covalent radii.<sup>10</sup> The indicated I–O bond is 2.30 Å in IBA(OH) (**6**, R = H)<sup>8</sup> and 2.35 Å in the derivative **6**, R = Me,<sup>9</sup> suggesting that the iodoxolone ring may be partially "open". Moreover, since it is the I–O<sup>-</sup> (anionic) form that is the active nucleophilic reagent, the bonding and electron distribution in the anion of IBA are also of great concern.



The X-ray structure of the sodium salt of 4-nitrosobenzoate, **7**, reveals an even larger endocyclic I–O bond length, 2.44 Å,<sup>9</sup> although how much of the additional "openness" should be attributed to an electron-withdrawing effect of the nitro group is unclear. Katritzky nevertheless concludes,<sup>9</sup> and we concur, that although the valence tautomerism between **1a** and **1b** lies "almost exclusively" on the closed, iodoxolone side, there is some contribution of the open, iodosocarboxylate form that might best be represented by a resonance hybrid featuring the "long" I–O bond and geometry of the iodoxolone, *cf.*, **8**. To the extent that iodoso structure **8b** contributes, further resonance delocalizes an electron pair over the lactone moiety (*cf.*, **8c**). Indeed, in the X-ray structure of anion **7**, the two lactone C–O bond lengths are nearly equal (1.251 and 1.259 Å),<sup>9</sup> whereas in the iodosobenzoic acid **6** (R = Me), the carbonyl C=O (1.24 Å) is somewhat shorter than the endocyclic C–O (1.28 Å).



Ab initio molecular orbital calculations carried out on **9**, the parent iodoxol-3(1H)-one, support the trends and conclusions elicited from the X-ray data.<sup>11</sup> Here, too, the (computed) endocyclic I–O distance increases (from 2.1 to 2.63 Å) upon deprotonation of **9** to anion **10**, while the lactone C–O distances (1.23 Å, C=O, vs 1.35 Å, C–O in **9**) approach equality (1.26 Å, C=O, vs 1.29 Å, C–O in **10**). However, despite the long endocyclic I–O bond in

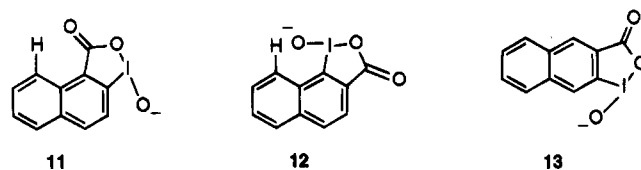


**10**, the anion is still best regarded as an iodoxolone.<sup>11</sup> In

particular, its computed *exocyclic* I–O<sup>-</sup> bond length, 1.92 Å, is far from the anticipated I=O bond length ( $\sim 1.6$  Å) of an iodosyl group and closer to that of an I–O single bond ( $\sim 2.07$  Å). Moreover, there is a large ab initio computed negative charge ( $-1.12$ ) on the O<sup>-</sup> of the *exocyclic* I–O in **10**, more consistent with an I–O<sup>-</sup> than an I=O part structure.<sup>11</sup>

The X-ray<sup>8,9</sup> and computational studies<sup>11</sup> indicate that the endocyclic I–O bonds in iodosocarboxylate anions are long and partly open, and as depicted in valence tautomer **1** and resonance hybrid **8**, the lactone unit relaxes toward a carboxylate.<sup>9,11</sup> To some extent, these structural features will decrease charge and nucleophilicity at I–O<sup>-</sup>, sapping reactivity toward P=O substrates. If, however, we could force the iodoxolone ring to "close", we might instead enhance these interconnected properties at I–O<sup>-</sup> and increase the nucleophilicity.

Accordingly, we prepared iodosonaphthoates **11–13**.<sup>12</sup> Planar models of **11** and **12** each displayed 8-*peri*-H/O separations of  $\sim 1.8$  Å, whereas the sum of the van der Waals radii was 2.6 Å. These steric interactions would be relieved if the iodoxolone rings closed somewhat at their endocyclic I–O bonds, simultaneously enhancing the negative charge at I–O<sup>-</sup>. Indeed, calculations suggested that the endocyclic I–O bond lengths of the iodosocarboxylates decreased in the order **10** > **1** > **11**, while the negative charge on O<sup>-</sup> increased in the reverse order (**11** greatest).<sup>12</sup>



In their reactivity toward PNPDP (2), **11** and **12** are 5–6 times more reactive than IBA but only  $\sim 25\%$  more reactive than iodosonaphthoate **13**, in which the *peri*-H steric interactions are absent.<sup>12</sup> These results are equivocal. The significant reactivity enhancement of the iodosonaphthoates, relative to IBA, can be largely attributed to the additional aromatic ring present in **11–13**, which affords greater hydrophobicity and better binding to the CTACl micelles on whose surface the reaction with PNPDP occurs; a comparable reactivity increase is also seen with a related iodosocarboxylate that has two aromatic rings but lacks the steric constraints of **11** and **12**.<sup>13</sup> However, the incremental reactivity advantage of **11** and **12** vs **13** might be a result of the former's steric interactions and suggests the additional test that is the subject of the present report.

Thus, 9,10-iodosphenanthroate, **14** (IPA), subsumes *both* of the *peri*-H/O interactions that are individually present in iodosonaphthoates **11** and **12**. Accordingly, the structure of IPA should be greatly distorted, relative to IBA, and its behavior toward PNPDP would constitute a significant test of the limits of reactivity modulation by the enforced structural modification of iodosocarboxylates. Here, we describe the synthesis, X-ray

(8) Shefter, E.; Wolf, W. *J. Pharm. Sci.* **1965**, *54*, 104.

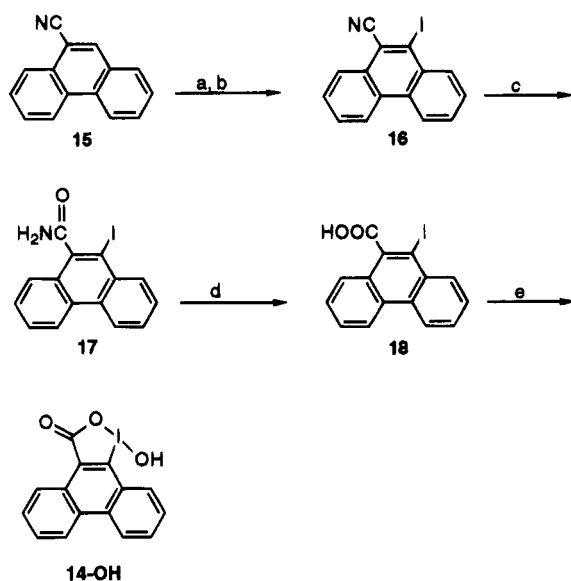
(9) Katritzky, A. R.; Savage, G. P.; Palenik, G. J.; Qian, K.; Zhang, Z.; Durst, H. D. *J. Chem. Soc., Perkin Trans. 2* **1990**, 1657.

(10) Pauling, L. *The Nature of the Chemical Bond*, 3rd ed.; Cornell University Press: Ithaca, NY, 1960; pp 221 f.

(11) Moss, R. A.; Wilk, B.; Krogh-Jespersen, K.; Blair, J. T.; Westbrook, J. D. *J. Am. Chem. Soc.* **1989**, *111*, 250.

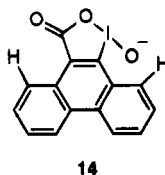
(12) Moss, R. A.; Zhang, H.; Chatterjee, S.; Krogh-Jespersen, K. *Tetrahedron Lett.* **1993**, *34*, 1729.

(13) Moss, R. A.; Zhang, H. *Tetrahedron Lett.* **1992**, *33*, 4291.

Scheme 1<sup>a</sup>

<sup>a</sup> Reagents and conditions: (a) LiTMP, THF,  $-78^{\circ}\text{C}$ , 1 h; (b)  $\text{I}_2$ ,  $-78$  to  $-25^{\circ}\text{C}$ , 2 h, 87% overall; (c) 3:2:1  $\text{H}_2\text{SO}_4$ , HOAc,  $\text{H}_2\text{O}$ , reflux, 9 h, 83%; (d)  $\text{NaNO}_2$ , 70% aqueous  $\text{H}_2\text{SO}_4$ ,  $25$ – $30^{\circ}\text{C}$ , 7 h, 78%; (e) *m*-CPBA,  $\text{CHCl}_3$ ,  $25^{\circ}\text{C}$ , 24 h, 79%.

crystal structure, and reactivity toward PNPDP of 9,10-iodosobenzoic acid.



## Results

**Synthesis.** The preparation of iodophenanthroic acid (14-OH, IPA-OH) is outlined in Scheme 1. The initial step, cyano-directed ortho lithiation and iodination of 9-cyanophenanthrene, 15,<sup>14</sup> to 9-cyano-10-iodophenanthrene, 16, was modeled after the analogous conversion of 1-cyanonaphthalene to 1-cyano-2-iodonaphthalene.<sup>15</sup> Thus, nitrile 15 was lithiated by lithium tetramethylpiperidide in THF at  $-78^{\circ}\text{C}$ , and the resulting 9-cyano-10-lithiophenanthrene was quenched with  $\text{I}_2/\text{THF}$  to afford iodo nitrile 16 in 87% yield. The composition of 16 was supported by IR, NMR, mass spectrometry, and elemental analysis. The structural adjacency of the nitrile and iodo substituents was signaled by the disappearance in iodo nitrile 16 of the  $\text{C}_{10}$  proton absorption at  $\delta$  8.67 (DMSO- $d_6$ ) of nitrile 15. The X-ray crystal structure of the 14-OH ultimately derived from 16 (see Scheme 1) secured this regiochemistry.

Iodo nitrile 16 could not be directly hydrolyzed to the desired iodo acid: Hydrolysis under basic conditions vigorous enough to effect the nitrile to carboxylate conversion led to loss of iodine, while similar problems attended overly strong acidic hydrolysis of 16. The successful approach involved partial hydrolysis of 16 to the corresponding amide 17 followed by the deamination of 17 to iodophenanthroic acid 18.

In practice, conditions that sufficed to convert 1-bromo-2-cyanonaphthalene to 1-bromo-2-naphthoic acid,<sup>16</sup> gave only iodo amide 17 from iodo nitrile 16. Thus, 9 h of gentle reflux (oil bath at  $120^{\circ}\text{C}$ ) of 16 in a 3:2:1 (by vol) blend of sulfuric acid, acetic acid, and water gave 83% of the iodo amide, whose structure was established by conventional means.

Deamination of 17 to iodo acid 18 was then accomplished by treatment with sodium nitrite in 70 wt % aqueous sulfuric acid,<sup>17</sup> yielding 78% of 18. IR spectroscopy (KBr) clearly reflected the 17  $\rightarrow$  18 conversion: The amide N–H ( $3433$  and  $3282\text{ cm}^{-1}$ ) and C=O ( $1658\text{ cm}^{-1}$ ) bands of 17 gave way to the OH ( $3405\text{ cm}^{-1}$ ) and C=O ( $1703\text{ cm}^{-1}$ ) bands of carboxylic acid 18.

The oxidation of iodo acid 18 to 9-iodosobenzoic acid, 14-OH, was achieved in 79% yield (44% overall yield from 15) using *m*-chloroperbenzoic acid (24 h at  $25^{\circ}\text{C}$ ).<sup>18</sup> Attempted oxidations with precedent reagents for the I  $\rightarrow$  I=O conversion, such as magnesium monoperoxyphthalate<sup>12,19</sup> or peracetic acid,<sup>20</sup> led to incomplete oxidation and low yields of IPA-OH.

The structure of IPA-OH was supported by IR spectroscopy, which revealed that the C=O stretch of 18 at  $1703\text{ cm}^{-1}$  had moved toward lower frequency ( $1649\text{ cm}^{-1}$ ) upon oxidation to 14-OH, in keeping with prior observations for analogous iodo to iodocarboxylic acid conversions.<sup>21–23</sup> The carbonyl bands of iodo acids, which normally appear above  $1660\text{ cm}^{-1}$ , fall in the  $1615$ – $1650\text{ cm}^{-1}$  range for the iodoso acids (iodoxolones) due to the partial ionic character of the long, endocyclic I–O bond and the partial “carboxylic acid” character of the lactone unit.<sup>23</sup> Additional structural support for 14-OH stemmed from the  $^1\text{H}$  NMR spectrum, where the I–OH proton appeared at  $\delta$  8.82 (DMSO- $d_6$ ), and from iodometric titration,<sup>24</sup> which afforded an iodoso titer of 100.4%, based on the assumption of purity.

**X-ray Crystal Structure.** Novel aspects of the IPA-OH structure were revealed by single-crystal X-ray analysis. Details of the data collection and structure solution appear in the Experimental Section. The final structure carried residual  $R(F) = 0.050$  and is shown in Figure 1. Selected bond lengths and angles are collected in Table 1.

The single-crystal X-ray diffraction results for 14-OH reveal a 1:1 stoichiometry of DMSO to IPA-OH. The unit cell packing is characterized by alternating sheets of segregated DMSO and iodoso molecules. In a given sheet of IPA-OH molecules, the somewhat flat portions of adjacent molecules are parallel and slightly overlapping in projection to the mean molecular plane. However, the  $\text{CO}_2\text{IOH}$  moieties of adjacent IPA-OH molecules are twisted out of their mean molecular planes and project

(16) Cirrigottis, K. A.; Ritchie, E.; Taylor, W. C. *Aust. J. Chem.* **1974**, *27*, 2209.

(17) Steinmetz, M. G.; Mayes, R. T. *J. Am. Chem. Soc.* **1985**, *107*, 2111. Tsai, L.; Miwa, T.; Newman, M. S. *Ibid.* **1957**, *79*, 2530.

(18) Hassner, A.; Reuss, R. H.; Pinnick, H. *J. Org. Chem.* **1975**, *40*, 3427.

(19) Brougham, P.; Cooper, M. S.; Cummerson, D. A.; Heaney, H.; Thompson, N. *Synthesis* **1987**, 1015.

(20) Sharefkin, J. G.; Saltzman, H. *Anal. Chem.* **1963**, *35*, 1428.

(21) Baker, G. P.; Mann, F. G.; Sheppard, N.; Tetlow, A. *J. Chem. Soc.* **1965**, 3721.

(22) Katritzky, A. R.; Savage, G. P.; Gallos, J. K.; Durst, H. *D. J. Chem. Soc., Perkin Trans. 2* **1990**, 1515.

(23) Ochiai, M.; Masaki, Y.; Shiro, M. *J. Org. Chem.* **1991**, *56*, 5511.

(24) Lucas, H. J.; Kennedy, E. R. In *Organic Synthesis*; Horning, E. C., Ed.; Wiley: New York, 1955; Collect. Vol. 3, pp 482–484. Vogel, A. I. *Quantitative Inorganic Analysis*; Wiley: New York, 1961; pp 343–359.

(14) 9-Cyanophenanthrene was purchased from Aldrich Chemical Co.

(15) Fraser, R. R.; Savard, S. *Can. J. Chem.* **1986**, *64*, 621.

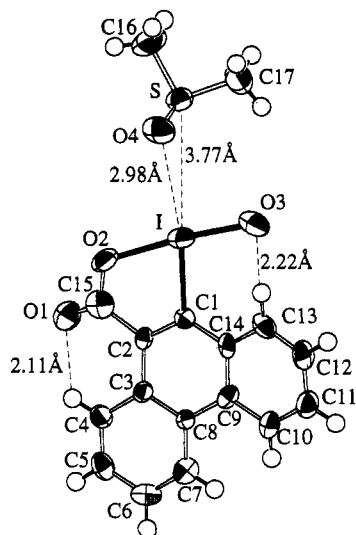


**Figure 1.** ORTEP diagram of the crystal structure of 14-OH showing nearest-neighbor DMSO and iodoso molecules. The thermal ellipsoids are plotted at the 50% probability level; H atoms are drawn as open spheres of arbitrary radii; intra- and intermolecular close contacts are shown as dashed lines; the H atom bonded to O<sub>3</sub> is not shown. See Table 1 for selected bond lengths and angles.

**Table 1. Selected Bond Lengths and Angles for 9-Iodoso-10-phenanthroic Acid, 14-OH<sup>a</sup>**

Bond Lengths (Å) <sup>b</sup>			
I-O <sub>3</sub>	1.993(10)	O <sub>1</sub> -C <sub>15</sub>	1.19(1)
I-O <sub>2</sub>	2.175(10)	O <sub>2</sub> -C <sub>15</sub>	1.32(2)
I-C <sub>1</sub>	2.149(11)	C <sub>2</sub> -C <sub>15</sub>	1.50(2)
C <sub>2</sub> -C <sub>1</sub>	1.35(1)	C <sub>8</sub> -C <sub>9</sub>	1.47(2)
C <sub>2</sub> -C <sub>3</sub>	1.46(2)	C <sub>1</sub> -C <sub>14</sub>	1.42(2)
Bond Angles (deg) <sup>b</sup>			
O <sub>3</sub> -I-C <sub>1</sub>	97.9(4)	C <sub>15</sub> -O <sub>2</sub> -I	114.7(11)
O <sub>3</sub> -I-O <sub>2</sub>	170.5(4)	O <sub>2</sub> -C <sub>15</sub> -C <sub>2</sub>	111.0(11)
O <sub>2</sub> -I-C <sub>1</sub>	76.2(4)	O <sub>1</sub> -C <sub>15</sub> -O <sub>2</sub>	125.0(2)
C <sub>2</sub> -C <sub>1</sub> -I	111.7(9)	C <sub>15</sub> -C <sub>2</sub> -C <sub>1</sub>	120.0(12)
C <sub>14</sub> -C <sub>1</sub> -I	122.4(8)	C <sub>14</sub> -C <sub>1</sub> -C <sub>2</sub>	125.8(11)
Torsion Angles (deg) <sup>b</sup>			
O <sub>3</sub> -I/O <sub>2</sub> -C <sub>15</sub>	29(3)	O <sub>3</sub> -I/C <sub>1</sub> -C <sub>2</sub>	-157.6(8)
O <sub>3</sub> -I/C <sub>1</sub> -C <sub>14</sub>	19.2(9)	I-C <sub>1</sub> /C <sub>14</sub> -C <sub>13</sub>	17.6(14)
I-C <sub>1</sub> /C <sub>2</sub> -C <sub>15</sub>	-7(2)	C <sub>15</sub> -C <sub>2</sub> /C <sub>3</sub> -C <sub>4</sub>	-2(2)
C <sub>1</sub> -I/O <sub>2</sub> -C <sub>15</sub>	-23.1(9)	C <sub>4</sub> -C <sub>3</sub> /C <sub>8</sub> -C <sub>7</sub>	2(2)
O <sub>1</sub> -C <sub>15</sub> /C <sub>2</sub> -C <sub>1</sub>	165(2)	C <sub>10</sub> -C <sub>9</sub> /C <sub>14</sub> -C <sub>13</sub>	-10(2)

<sup>a</sup> See Figure 1 for numbering of the atoms. <sup>b</sup> Numbers in parentheses are estimated standard deviations in the least significant digit. Bond geometry esds are somewhat high due to the relatively low data:parameter ratio (1235:209).

in a stepwise fashion into the interface between the sheets of the DMSO and IPA-OH molecules. Also within this interface, the S-O vector of each DMSO molecule is directed toward one I atom. In this way, several close contacts are found between a given IPA-OH molecule and four neighboring DMSO molecules across the interface. The closest contacts are between the IPA-OH I atom and S and O<sub>4</sub> of a DMSO molecule; see Figure 1.

The H atom bonded to O<sub>3</sub> of 14-OH could not be located with high precision. However, the restrained refinement (see the Experimental Section) of this atom, HO<sub>3</sub>, did converge to a good O-I/O-H torsion angle (*i.e.*, no new unfavorable steric interactions resulted), such that the angle involving the H<sub>13</sub>...O<sub>3</sub> intramolecular contact, namely, H<sub>13</sub>...O<sub>3</sub>-HO<sub>3</sub>, was 120(1)°.

Highlights of the molecular structure of IPA-OH in Figure 1 include the expected<sup>7</sup> T-shaped geometry at

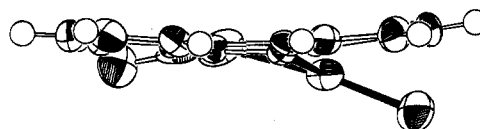


**Figure 2.** ORTEP diagram of an edge-on view of 14-OH. The thermal ellipsoids are plotted at the 50% probability level; H atoms are drawn as open spheres of arbitrary radii. The view is approximately along the C<sub>2</sub>-O<sub>2</sub> vector.

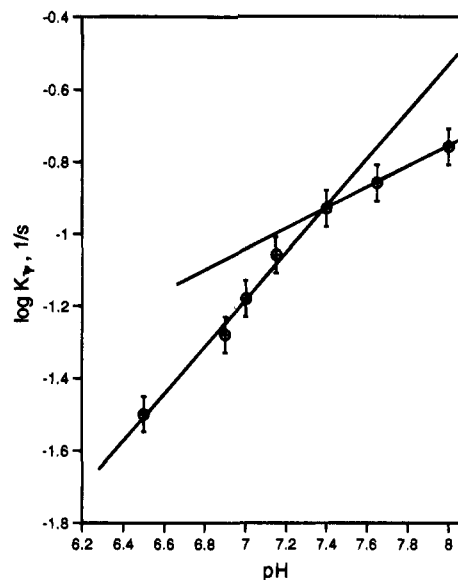


**Figure 3.** pH-rate profile for the cleavage of  $1 \times 10^{-5}$  M PNPDP by  $1 \times 10^{-4}$  M IPA-OH in  $1 \times 10^{-3}$  M micellar CTACl;  $\log k_p$  ( $s^{-1}$ ) vs pH. The discontinuity at pH 7.4 is taken as the systemic  $pK_a$ . See text for details of the reaction conditions.

iodine (O<sub>2</sub>-I-O<sub>3</sub> = 170.5°), strong H/O steric interactions between the H atoms at C<sub>4</sub> and C<sub>13</sub> and the carbonyl (O<sub>1</sub>) and iodoso (O<sub>3</sub>) oxygen atoms, a "short" (2.17 Å) endocyclic I-O<sub>2</sub> bond, well-differentiated carbonyl (C<sub>15</sub>-O<sub>1</sub>) and endocyclic (C<sub>15</sub>-O<sub>2</sub>) C-O bond distances, and, most impressively, nonplanarity of *both* the iodoxolone and phenanthrene rings. This novel feature is clearly shown in the edge-on view of 14-OH that appears in Figure 2, where the phenanthrene is closest to the viewer and the I-O bond extends downward at the right lower rear of the ORTEP view.

**pK<sub>a</sub> Determination.** The apparent  $pK_a$  of IPA-OH was obtained from a pH-rate constant profile<sup>3</sup> for the cleavage of  $1 \times 10^{-5}$  M PNPDP by  $1 \times 10^{-4}$  M IPA-OH in  $1 \times 10^{-3}$  M micellar CTACl in 0.02 M aqueous phosphate buffer,  $\mu = 0.08$  (NaCl), at 25 °C. The buffer solution also contained 1.0 vol % DMSO and 0.33 vol % MeCN as residuals from reagent additions.

Pseudo-first-order rate constants for PNPDP cleavage were determined from the time dependent release of *p*-nitrophenol/*p*-nitrophenylate monitored at 400 nm. A plot of  $\log k_p$  vs pH at 7 pH values, over the range 6.5–8.0, gave Figure 3, where the discontinuity at pH 7.4 is taken as the systemic  $pK_a$  of IPA-OH under the micellar reaction conditions.<sup>25</sup> The  $pK_a$  determined for IPA-OH is typical of related iodoxolones under cationic micellar conditions. Comparable data for 1, 9, and 11–13 are 7.25,<sup>3a</sup> 7.78,<sup>11</sup> 7.70,<sup>12</sup> 7.20,<sup>12</sup> and 7.10,<sup>12</sup> respectively. Under our "standard" kinetic conditions for the determination of optimal iodoxolone reactivity at pH 8, a  $pK_a$  of

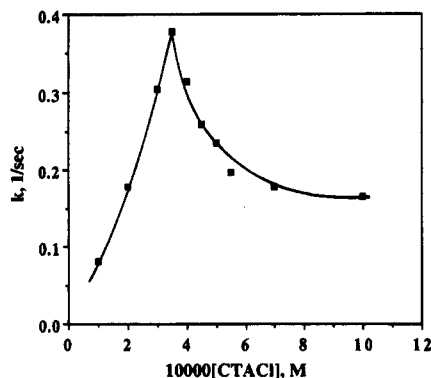


**Figure 4.** Pseudo-first-order rate constants ( $k_p$ ,  $s^{-1}$ ) for the cleavage of  $1 \times 10^{-5}$  M PNPDP by  $1 \times 10^{-4}$  M IPA-OH as a function of CTACl concentration at pH 8.0. See text for details of the reaction conditions;  $k_p(\text{max})$  is  $0.38 \text{ s}^{-1}$  at  $[\text{CTACl}] = 3.5 \times 10^{-4}$  M.

7.4 means that IPA-OH will be  $\sim 80\%$  ionized to its reactive, anionic IPA (**14**) form.

**Reactivity.** The catalytic properties of IPA were assessed from a full rate constant-[surfactant] profile for the cleavage of  $1 \times 10^{-5}$  M PNPDP by  $1 \times 10^{-4}$  M IPA at  $25^\circ\text{C}$ , under the buffer conditions described above. The CTACl concentration was incrementally varied between  $1 \times 10^{-4}$  and  $1 \times 10^{-3}$  M, and 10 pseudo-first-order rate constants were determined by monitoring *p*-nitrophenylate release at 400 nm with an OLIS RSM-1000 stopped-flow spectrometer. The reproducibility of  $k_p$  was better than  $\pm 3\%$  in duplicate runs.

The data appear in Figure 4, where  $k_p(\text{max}) = 0.38 \text{ s}^{-1}$  at  $[\text{CTACl}] = 3.5 \times 10^{-4}$  M. The correlation resembles other examples of micellar catalysis<sup>26a</sup> and applies to oxido-iodoxolone cleavages catalyzed by a micellar surfactant; related profiles were observed with (*e.g.*) IBA,<sup>3b</sup> the parent iodoxolone **10**,<sup>11</sup> and iodosonaphthoates **11** and **13**.<sup>12,27</sup> In Figure 4, the rate constant increases rapidly as the IPA and PNPDP are bound by the CTACl micelles, reaches a maximum when the binding is optimal, and then declines as additional surfactant dilutes the micellar pseudophase in which the reaction takes place. It is of interest that the CTACl concentration ( $3.5 \times 10^{-4}$  M) at which  $k_p(\text{max})$  is observed for IPA-OH is slightly lower than the analogous concentration ( $5.0 \times 10^{-4}$  M) for the iodosonaphthoate catalysts.<sup>12</sup> Presumably, this reflects stronger binding of the more hydrophobic IPA catalyst.

We should note, however, that since the CTACl concentration at  $k_p(\text{max})$  is only 3.5 times greater than the IPA concentration, it is unlikely that typical CTACl micelles are present. Thus, if the aggregation number of the micelles is 50, there would be  $\sim 14$  IPA molecules for each CTACl micelle. Most likely, therefore, we are dealing with mixed aggregates of IPA and CTACl, premi-

**Table 2.** Turnover Experiments with IPA-OH and PNPDP<sup>a</sup>

run	$10^5$ cumulative [PNPDP] (M)	total PNPDP (equiv)	$k_p$ ( $s^{-1}$ )
1	2.0	0.2	0.17
2	4.0	0.4	0.20
3	6.0	0.6	0.15
4	8.0	0.8	0.15
5	10.0	1.0	0.15
6	12.0	1.2	0.15
7	14.0	1.4	0.12
8	20.0	2.0	0.091
9	30.0	3.0	0.048

<sup>a</sup> See text for concentrations and conditions.

**Table 3.** Kinetics of Iodosocarboxylate Cleavages of PNPDP (**2**)<sup>a</sup>

catalyst	$pK_a^b$	$k_p(\text{max})$ ( $s^{-1}$ ) <sup>c</sup>	$10^3[\text{CTACl}]$ (M) <sup>d</sup>	$k_{\text{cat}}$ ( $M^{-1} \text{ s}^{-1}$ ) <sup>e</sup>	$k_{\text{turn}}$ ( $s^{-1}$ ) <sup>f</sup>	ref
<b>10</b>	7.78	0.010	3.00	160		<i>g</i>
<b>1b</b>	7.25 <sup>h</sup>	0.064	1.00	759	0.024 <sup>i</sup>	<i>j</i>
<b>11</b>	7.70	0.31	0.50	4660	0.10	<i>k</i>
<b>12</b>	7.20	0.36	0.50	4190	0.23	<i>k</i>
<b>13</b>	7.10	0.26	0.50	2950	0.16	<i>k</i>
<b>14</b>	7.40	0.38	0.35	4750	0.091	<i>l</i>

<sup>a</sup> Conditions: 0.02 M pH 8.0 phosphate buffer,  $\mu = 0.08$  (NaCl),  $25 \pm 0.5^\circ\text{C}$ ,  $[\text{PNPDP}] = 1 \times 10^{-5}$  M,  $[\text{catalyst}] = 1 \times 10^{-4}$  M, 1.0 vol % DMF, 0.33 vol % MeCN. The formation of *p*-nitrophenylate ion was followed at 400 nm. <sup>b</sup> Determined from pH-rate constant profiles for the cleavage of PNPDP in micellar CTACl. <sup>c</sup> Maximum pseudo-first-order rate constant for PNPDP cleavage taken from rate constant/[CTACl] profile. <sup>d</sup> Concentration of CTACl at which  $k_p(\text{max})$  was observed. <sup>e</sup>  $k_{\text{cat}} = k_p(\text{max})/[\text{catalyst}]$ , corrected for 100% ionization to  $\text{IO}^-$ ;  $pK_a$  values are given in the table. <sup>f</sup> Pseudo-first-order rate constant for cleavage of 2-fold excess PNPDP in  $1 \times 10^{-3}$  M CTACl; other conditions were as in footnote a. <sup>g</sup> Reference 11. <sup>h</sup> *p*-Nitrophenyl acetate was the substrate.<sup>3a</sup> <sup>i</sup> 5-Fold excess PNPDP,  $1 \times 10^{-2}$  M CTACl.<sup>3a</sup> <sup>j</sup> References 3a, b. <sup>k</sup> Reference 12. <sup>l</sup> This work.

cellar CTACl aggregates, hydrophobic IPA/CTACl ion pairs, or combinations of these entities, each of which can be expected to be kinetically potent.<sup>26b</sup>

**Turnover.** To test the ability of IPA to cleave excess substrate, the following set of experiments was performed. A solution of  $1 \times 10^{-4}$  M IPA in  $1 \times 10^{-3}$  M CTACl at pH 8, under our standard buffer conditions, was sequentially treated with  $>0.2$  equiv portions of PNPDP. After each addition of substrate, the cleavage kinetics were followed to completion, and the theoretical quantity of *p*-nitrophenylate ion was observed. These experiments were continued until a total of 3.0 mol equiv of PNPDP had been added. The data appear in Table 2, where all of the rate constants obeyed strict first-order kinetics.

The relatively invariant  $k_p$  observed for successive cleavages of PNPDP, up to  $\sim 1.4$  mol equiv of substrate, indicates that the IPA "turns over" during each cycle and is again present at its initial concentration, ready to react with the next sample of substrate.<sup>28</sup> After 2.0 equiv of PNPDP was added, however,  $k_p$  decreased by  $\sim 40\%$ , an effect noted in experiments with other iodoxolones (see below; Table 3). The retarding effect is even more pronounced at 3 equiv of substrate. The retardations may be due to binding of the liberated *p*-nitrophenylate

(25) The pH-rate constant profile method for the estimation of  $pK_a$  resembles the approach used in enzymology. For the relevant discussion, see: Laidler, K. J. *Chemical Kinetics*, 3rd ed.; Harper & Row: New York, 1987; pp 406–409. The conclusion that the pH value at which the two lines intersect equals the  $pK_a$  can be readily derived from the definition of  $K_a$  and the rate law. We estimate the error in the  $pK_a$  to be  $\pm 0.1$ .

(26) (a) Fendler, J. H.; Fendler, E. J. *Catalysis in Micellar and Macromolecular Systems*; Wiley: New York, 1975; Chapter 5, pp 104 f. (b) Fendler, J. H. *Membrane Mimetic Chemistry*; Wiley: New York, 1982; pp 35 f.

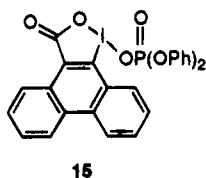
(27) (a) Zhang, H. Ph.D. Dissertation, Rutgers University, New Brunswick, NJ, 1993; p 50. (b) Chatterjee, S. Ph.D. Dissertation, Rutgers University, New Brunswick, NJ, 1990; p 33.

(28) Note that  $k_p = 0.15\text{--}0.20 \text{ s}^{-1}$  at  $[\text{CTACl}] = 1.0 \times 10^{-3}$  M, which is considerably slower than  $k_p(\text{max}) = 0.38 \text{ s}^{-1}$  at  $[\text{CTACl}] = 3.5 \times 10^{-4}$  M;  $k_p$  decreases at higher CTACl concentrations (see Figure 4). At  $1 \times 10^{-3}$  M CTACl, the bimolecular rate constant for IPA/PNPDP cleavage is  $830 \text{ M}^{-1} \text{ s}^{-1}$ , as determined from the slope of a correlation of  $k_p$  with  $[\text{IPA}]$  for the cleavage of  $2 \times 10^{-4}$  M PNPDP.

ions to the CTACl micelles, where they compete with substrate and/or IPA, reduce their partition into the micellar phase, and slow the reaction. Alternatively, the micelles themselves may be further altered in the presence of substantial *p*-nitrophenylate.

Supporting these interpretations is a control experiment in which  $1.2 \times 10^{-4}$  M *p*-nitrophenylate was added to  $1.0 \times 10^{-4}$  M IPA in  $1.0 \times 10^{-3}$  M CTACl at pH 8 to partially simulate the conditions at the end of run 6 (Table 2). Subsequent additions of 0.2 and 0.5 equiv of PNPDPF then produced cleavage rate constants of 0.11 and  $0.096 \text{ s}^{-1}$ , experimentally identical with the results of runs 7 and 8 for the cumulative cleavages of PNPDPF.

Nevertheless, maintenance of strict first-order kinetics in each of the reactions of Table 2 shows that IPA does turn over after reaction with PNPDPF; it is not "tied up" as a stable phosphorylated IPA (15). Rather, as in the case of phosphorylated IBA 5,<sup>6</sup> intermediate 15 must hydrolyze rapidly at pH 8.



### Discussion

**Structure.** Our intent in the construction of IPA was to use the structurally enforced steric interactions between the *peri*-H atoms and the carbonyl and I-O<sup>-</sup> oxygen atoms to force the iodoxolone ring to "close", shortening the endocyclic I-O bond and, presumably, increasing electron density on the oxido oxygen. The X-ray crystal structure of IPA-OH (see Figures 1 and 2 and Table 1) indicates that we have succeeded. Indeed, we may have succeeded too well; not only has the desired I-O bond been shortened, but the entire structure has buckled, with nonplanarity evident in both the iodoxolone ring and the phenanthrene scaffold.

Figure 1 and Table 1 indicate that IPA-OH, like IBA-OH, is cyclized to an iodoxolone.<sup>7-9</sup> One can imagine approximate trigonal bipyramidal geometry around iodine, with O<sub>3</sub> and O<sub>2</sub> at the apical positions and the three equatorial positions occupied by C<sub>1</sub> and two lone electron pairs on iodine. With an O<sub>3</sub>-I-O<sub>2</sub> bond angle of 170.5°, IPA-OH exhibits the T-shaped coordination geometry expected around the formally hypervalent iodine atom.<sup>7</sup> The large deviation from a regular pentagonal bond angle (108°) found at the O<sub>2</sub>-I-C<sub>1</sub> bond angle (76.2°) permits the other angles in the iodoxolone ring to relax to near-ideal values (112–120°).<sup>29</sup>

Of key interest are the I-O and C-O bond lengths of the iodoxolone ring. For brevity, comparisons are restricted to our structure for IPA-OH and Katritzky's structure for 5-methyl-2-iodosobenzoic acid (6, R = Me),<sup>9</sup> the only other recent crystal structure for an I-OH iodoxolone.<sup>30</sup> The key endocyclic I-O bond in IPA-OH (I-O<sub>2</sub>) is 2.17 Å, ~0.18 Å shorter than the comparable I-O bond in 6, R = Me (2.35 Å), even though the former is still 0.1 Å longer than the 2.07 Å sum of I and O single bond covalent radii.<sup>10</sup> This shortening is most likely a

consequence of the *peri*-H/O steric repulsions shown in Figure 1. The observed H/O<sub>1</sub> and H/O<sub>3</sub> separations of ~2.2 Å (calculated with C-H distances of 1.08 Å) are well within the 2.6 Å sum of the H/O van der Waals radii. Contraction of the I-O<sub>2</sub> bond is one way of relieving these repulsions, although bond angle distortion also absorbs much of the strain (see below).

The endocyclic I-O contraction is complemented by a slight lengthening of the exocyclic I-O<sub>3</sub> bond (1.99 vs 1.94 Å in 6, R = Me), suggesting less "double-bond" character in the exocyclic I-O of IPA-OH and, possibly, more electron density on the oxygen.

Finally, closure of the endocyclic I-O bond in IPA-OH should result in greater differentiation of the carbonyl and endocyclic C-O bond lengths in the lactone portion of the iodoxolone ring. Indeed, these bonds [1.19 Å for C=O (C<sub>15</sub>-O<sub>1</sub>) and 1.32 Å for C<sub>15</sub>-O<sub>2</sub>] are more differentiated than the analogous C=O and C-O bonds in 6, R = Me, which are 1.24 and 1.28 Å, respectively.<sup>9</sup>

The structural constraints imposed on IPA-OH do lead to the desired shortening of the endocyclic I-O bond, but much of the strain is also absorbed by bond angle distortions that lead to a marked loss of planarity. Although the unconstrained iodobenzoic acids 6, R = H or Me, are planar,<sup>7-9</sup> IPA-OH is nonplanar in both the iodoxolone and phenanthrene rings; *cf.*, Table 1 and Figure 2. The I-OH end of the iodoxolone is distorted by 19.2° from the average plane of the phenanthrene, while the iodoxolone ring itself, as represented by the C<sub>1</sub>-I/O<sub>2</sub>-C<sub>15</sub> dihedral angle, is distorted from planarity by ~23°. There is also a 10° out-of-plane bending within the phenanthrene ring, with C<sub>12</sub> and C<sub>13</sub> bent up from C<sub>9</sub> and C<sub>10</sub> because of their interaction with the I-OH oxygen atoms and the C<sub>13</sub> H atom.

IPA-OH is the first iodoxolone observed to be nonplanar. Of course, the *peri*-H/O interactions in naphthoates 11 and 12 might also induce nonplanarity in their iodoxolone rings, but their crystal structures are not available.

We believe that the general features of interest described for IPA-OH in the crystal largely persist for anionic IPA (14) in solution. The endocyclic I-O bond appears to lengthen upon ionization of I-OH to I-O<sup>-</sup> in unconstrained systems,<sup>9,11</sup> and, in 14, this tendency would likely maintain the steric repulsions built into 14-OH. Thus, the imposed I-O contraction should persist in oxidoiodoxolone 14 in solution, relative to the unconstrained iodobenzoates, even though we lack a precise measure of the contraction; it could be more or less than the 0.17 Å observed in the IPA-OH vs 6, R = Me, crystal structures.

**Reactivity of IPA.** In Table 3, we collect kinetic data for IPA (14), the parent oxidoiodoxolone 10,<sup>11</sup> IBA (1b),<sup>3a,b</sup> and the three isomeric naphthiodoxolones 11–13.<sup>12</sup> In addition to the pK<sub>a</sub>, k<sub>v</sub>(max) for PNPDPF cleavage, and the concentration of CTACl necessary to elicit k<sub>v</sub>(max), Table 3 also includes "k<sub>cat</sub>," defined as k<sub>v</sub>(max)/[catalyst], corrected to 100% ionization of the I-OH, using the cited pK<sub>a</sub> value at pH 8. The k<sub>cat</sub> data permit direct reactivity comparisons of the several iodocarboxylates. Finally, we include "k<sub>turn</sub>," a measure of the turnover efficiency of the iodoxolones, taken as k<sub>v</sub> for the cleavage of a 2-fold excess of PNPDPF by 1 × 10<sup>-4</sup> M catalyst in 1 × 10<sup>-3</sup> M CTACl.<sup>28</sup> From the k<sub>v</sub>(max) and k<sub>cat</sub> data, IPA is seen to be an extremely potent reagent for the cleavage of PNPDPF. The turnover data show that IPA is also a true catalyst, able to cleave excess substrate.

(29) Koser, G. F.; Wettach, R. H.; Troup, J. M.; Frenz, B. A. *J. Org. Chem.* 1976, 41, 3609.

(30) Katritzky points out<sup>9</sup> that the 1965 structure reported for iodobenzoic acid itself<sup>9</sup> is "of low accuracy".

Despite these positive findings, however, IPA proves to be little more reactive than the angularly substituted naphthiodoxolone **11**. Whatever additional negative charge is forced onto the I-O<sup>-</sup> of IPA by dint of its steric constraints and shortened endocyclic I-O bond may be undercut by the serious congestion at I-O<sup>-</sup>, which results in nonplanarity of both the iodoxolone and phenanthrene. The congestion may also result in steric hindrance to attack by the I-O<sup>-</sup> on PNPDP, a relatively large substrate molecule. Moreover, intermediate **15**, derived by phosphorylation of **14**, must be even more strained. Its energy and the activation energy leading to it will be elevated, further eroding any kinetic advantage.

Comparisons of  $k_{cat}$  for iodoxolones **10**, **1b**, and **11** indicate significant reactivity enhancements with each additional aromatic ring in the catalyst, an observation previously attributed to greater catalyst hydrophobicity, enhanced micellar binding, and more efficient reaction with the hydrophobic, micelle-bound PNPDP.<sup>12</sup> In this light, the failure of IPA, which contains three aromatic rings, to exhibit greater reactivity than **11** underscores the inability of the additional steric interactions present in IPA to translate into significant kinetic advantage. However, the structural changes induced by the steric interactions built into IPA-OH remain dramatic and novel.

## Experimental Section

**General Methods.** All reactions of air- and moisture-sensitive compounds were carried out in dry reaction vessels under nitrogen. Samples were introduced either neat or in organic solvent via syringe through rubber septa. Teflon tape was used to seal joints in the apparatus.

Melting points were taken on a Mel-Temp apparatus in open capillary tubes and are uncalibrated. Spectra were recorded on the following spectrometers: Varian XL-200 (200 MHz, <sup>1</sup>H NMR), ATI Mattson Genesis Series (FTIR), Hewlett Packard 5890 Series II (GC/MS). Chemical shifts ( $\delta$ ) are reported relative to tetramethylsilane. Microanalyses were performed by Quantitative Technologies, Inc., Whitehouse, NJ.

**Materials.** PNPDP was prepared and purified by literature methods.<sup>31</sup> CTACI was purchased from Eastman Kodak and purified by recrystallization three times from methanol/ether. Commercially available chemicals were used as received without further purification unless otherwise noted. THF was dried by refluxing over sodium/benzophenone ketyl and freshly distilled prior to use. Methylene chloride was dried by successive distillations over P<sub>2</sub>O<sub>5</sub> and K<sub>2</sub>CO<sub>3</sub> and stored over molecular sieves.

**9-Cyano-10-iodophenanthrene (16).** This procedure could be successfully carried out on 1–15 g samples of 9-cyanophenanthrene (**15**). For example, 1.66 mL (9.8 mmol) of 2,2,6,6-tetramethylpiperidine was added by syringe to 40 mL of freshly distilled THF in a dried round bottom flask, equipped with a nitrogen gas inlet and rubber septum, and maintained under an atmosphere of nitrogen. This solution was cooled to 0 °C with an ice-salt bath. Next, 9.1 mL (12.7 mmol) of 1.4 M methylolithium in diethyl ether was added dropwise by syringe. After stirring at 0 °C for 30 min, the yellow-green solution was cooled to -78 °C, and a solution of 2.0 g (9.8 mmol) of 9-cyanophenanthrene (**15**) in 15 mL of dry THF was added dropwise by syringe; the solution was stirred at -78 °C for 1 h. The resulting ortho-lithiated **15** was quenched by syringe addition of a solution of 2.49 g (9.81 mmol) of I<sub>2</sub> in dry THF followed by gradual warming to room temperature over 2 h. The resulting deep maroon mixture was slowly poured into an excess of water at 15 °C, with vigorous stirring, to give a crude orange product, which was filtered and treated with

decolorizing carbon in boiling chloroform. We thus obtained 2.8 g (8.5 mmol, 87%) of pale cream-colored flakes: mp 219–220 °C; IR (KBr) 2218 cm<sup>-1</sup> (C≡N); <sup>1</sup>H NMR (DMSO-*d*<sub>6</sub>)  $\delta$  7.83–7.93 (m, 4 H), 8.18 (d of d,  $J = 4$ , 2 Hz, 1 H), 8.32 (d of d,  $J = 4$ , 2 Hz, 1 H), 8.94 (t,  $J = 8$  Hz, 2 H); MS M<sup>+</sup> at *m/e* 329. Anal. Calcd for C<sub>15</sub>H<sub>9</sub>IN: C, 54.7; H, 2.45; N, 4.26; I, 38.6. Found: C, 54.9; H, 2.35; N, 4.20; I, 38.2.

**9-Carboxamido-10-iodophenanthrene (17).** Iodo nitrile **16** (0.60 g, 1.8 mmol) was combined with 6 mL of water and 12 mL of glacial acetic acid. Then, 18 mL of concentrated sulfuric acid was added in small portions over 30 min. The resulting mixture was refluxed (oil bath at 120 °C) for 9 h, allowed to cool, and then poured into 0.8 L of cold water, with vigorous stirring, to give an off-white powder which was filtered under vacuum suction. After treatment with decolorizing carbon in boiling CHCl<sub>3</sub>, we obtained 0.53 g (1.5 mmol, 83%) of iodo amide **17** as a white powder, mp 120 °C dec; IR (KBr) 3433, 3282, 1658 cm<sup>-1</sup>; <sup>1</sup>H NMR (DMSO-*d*<sub>6</sub>)  $\delta$  7.69–7.80 (m, 4 H), 7.89 (d,  $J = 4$  Hz, 1 H), 7.97 (br s, 1 H, NH), 8.16 (br s, 1 H, NH), 8.29–8.34 (m, 1 H), 8.84–8.92 (m, 2 H); MS M<sup>+</sup> at *m/e* 347. Anal. Calcd for C<sub>15</sub>H<sub>10</sub>INO·H<sub>2</sub>O: C, 49.3; H, 3.31; N, 3.84. Found: C, 49.2; H, 2.96; N, 4.03.

**9-Iodo-10-phenanthroic Acid (18).** The iodo amide **17** (100 mg, 0.288 mmol) was dissolved with heating in 2.5 mL of acetonitrile. Next, 12.5 mL of chilled 70% (w/w) sulfuric acid was slowly added. After the solution had cooled to 30 °C, 200 mg (2.90 mmol) of solid sodium nitrite was added in small portions over 1 h. Gas evolution and a color change to red-brown was accompanied by the formation of a pale yellow precipitate during the course of the addition. This mixture was allowed to stir in the dark at room temperature for 6 h and then poured onto ice. The precipitate was filtered, washed with cold water, and dried to give 78 mg (0.22 mmol, 78%) of iodophenanthroic acid: mp 196–198 °C; IR (KBr) 3405, 1703 cm<sup>-1</sup>; <sup>1</sup>H NMR (DMSO-*d*<sub>6</sub>)  $\delta$  7.71–7.82 (m, 5 H), 8.26–8.31 (m, 1 H), 8.85–8.95 (m, 2 H). Anal. Calcd for C<sub>15</sub>H<sub>9</sub>IO<sub>2</sub>: C, 51.7; H, 2.61. Found: C, 50.7; H, 2.60. This was the best of several analyses. Difficulty was experienced in removing traces of amide **17**, and elemental analysis revealed 0.66% N. The structure of acid **18** is confirmed by the X-ray analysis of the derived iodoso acid **14-OH**.

**9-Iodoso-10-phenanthroic Acid (14-OH).** Iodo acid **18** (100 mg, 0.287 mmol) was suspended in 2.5 mL of CHCl<sub>3</sub> and stirred. Then 70 mg (0.40 mmol) of *m*-chloroperbenzoic acid (85%; Aldrich) was added, and the mixture was stirred in the dark at ambient temperature. After 2 h, a yellow-gold precipitate began to form. After 24 h, 30 mL of saturated aqueous sodium bicarbonate solution was added, and stirring was continued for 30 min. The yellow iodoso product was filtered under vacuum and washed with cold water to give 84 mg (0.23 mmol, 79%) of the yellow iodosophenanthroic acid: mp 158 °C dec; IR (KBr) 3427, 1649 cm<sup>-1</sup>; <sup>1</sup>H NMR (DMSO-*d*<sub>6</sub>)  $\delta$  7.70–7.93 (m, 4 H), 8.82 (s, 1 H, I-OH, exchanges with D<sub>2</sub>O), 8.97 (crude t,  $J = 8$  Hz, 2 H), 9.23 (d,  $J = 8$  Hz, 1 H), 9.80–9.85 (m, 1 H). Iodometric titration<sup>24</sup> gave 100.4% of I=O.

**X-Ray Structure Determination.** The crystal used for the X-ray data collection of **14-OH** was a colorless prism of dimensions 0.025 × 0.10 × 0.20 mm<sup>3</sup>, obtained from a supersaturated solution in DMSO. Intensity data were collected on an Enraf-Nonius CAD4 diffractometer using graphite monochromatized Mo K $\alpha$  ( $\lambda = 0.71069$  Å) radiation at room temperature. A set of 25 reflections with 12° <  $\theta$  < 14° were used to determine the unit cell data for **14-OH**: space group C2 (no. 5);  $Z = 4$ ;  $a = 33.741(4)$  Å;  $b = 5.277(1)$  Å;  $c = 9.120(2)$  Å;  $\beta = 101.89(2)^\circ$ ;  $V = 1589.0(5)$  Å<sup>3</sup>. For a formula weight of 442.25 for **14-OH**·DMSO (C<sub>17</sub>H<sub>15</sub>IO<sub>4</sub>S), the density was calculated to be 1.849 g cm<sup>-3</sup>. Of the 1332 reflections collected in the  $\theta$  range 2–23°, there were 1235 independent data, of which 1081 were observed to have  $I > 2\sigma(I)$ . A numerical absorption correction<sup>32</sup> was applied to the data. The structure of **14-OH** was solved by Patterson methods,<sup>33</sup> was refined (209 param-

(31) Gulick, W. M., Jr.; Geske, D. H. *J. Am. Chem. Soc.* **1966**, *88*, 2928.

(32) Sheldrick, G. M. *SHELX76. Program for Crystal Structure Determination*; University of Cambridge: Cambridge, England, 1976.

eters varied) based upon all 1235  $F^2$  data,<sup>34</sup> and resulted in the following residuals:  $R(F) = 0.050$  [0.038 for  $I > 2\sigma(I)$ ];  $R_w(F^2) = 0.077$  [0.073 for  $I > 2\sigma(I)$ ]; GOF = 1.002; final difference Fourier map excursions of  $-0.4$ – $0.7$  e  $\text{\AA}^{-3}$ . The Flack parameter<sup>35</sup> for absolute structure was  $-0.03(6)$ . The aromatic and methyl H atoms were placed in calculated positions with C–H distances of 0.93 and 0.96  $\text{\AA}$ , respectively. Of the several significant difference Fourier map peaks ( $0.3$ – $0.7$  e  $\text{\AA}^{-3}$ ) in the vicinity of  $O_3$  in **14**-OH and  $O_4$  in DMSO, one was selected as the H atom bonded to  $O_3$ , namely,  $H_3$ , which was given a fixed O–H distance (0.82  $\text{\AA}$ ), a fixed I–O–H angle ( $109.5^\circ$ ), and a refined O–I/O–H torsion angle.

**Kinetic Studies.** Reactions with  $\tau_{1/2} < 10$  s were followed on an OLIS RSM 1000 UV/vis stopped-flow spectrophotometer coupled to a 486/66 MHz computer with VGA graphics. Slower reactions, turnover reactions, and  $pK_a$  kinetics were followed on a Gilford Model 250 spectrophotometer coupled to a Servogor Model 120 chart recorder. Constant-temperature circulating baths were used to maintain reaction temperatures at  $25 \pm 0.5$  °C. All buffers were prepared from "steam-

distilled" water (distilled, U.S.P.; Electrified Water Co., East Orange, NJ). Pseudo-first-order rate constants were obtained from computer-generated correlations of  $\log(A_\infty - A_t)$  versus time for the appearance of *p*-nitrophenoxide ion at 400 nm using Sigma Plot software. Conditions for all kinetic runs are described under Results. Micellar reactions were generally followed to >95% completion and showed good first-order kinetics ( $R > 0.997$ ). Reproducibility of the rate constants was  $\pm 3\%$  in duplicate runs. Rate constants for the title compound and related compounds are tabulated in Table 3. The [CTAC]–rate constant profile is presented graphically in Figure 4; the pH–rate constant profile appears in Figure 3. Turnover kinetics are collected in Table 2. Conditions for all of the kinetic runs are described under Results.

**Acknowledgment.** We are grateful to the U.S. Army Research Office for general financial support. Additionally, K.B. acknowledges a stipend from an AASERT grant from the U.S. Army Research Office. We thank Dr. Brian T. Buckley and Mr. Wei Fang (Environmental and Occupational Health Sciences Institute, Rutgers University) for use of the stopped-flow spectrophotometer. We also thank Professors R. R. Sauers and L. S. Romsted for helpful discussions.

JO951202U

(33) Sheldrick, G. M. *SHELXS86. Program for the Solution of Crystal Structures*; University of Göttingen: Göttingen, Germany, 1986.

(34) Sheldrick, G. M. *SHELXL93. Program for Crystal Structure Refinement*; University of Göttingen: Göttingen, Germany, 1993. Residuals (*R*-factors) and weights (*w*) are defined therein.

(35) Flack, H. D. *Acta Crystallogr.* **1983**, *A39*, 876.